Multi-Response Optimization of Process Parameters in Friction Stir Welding of AA 8011-H14 / AA 5052-H34 using Taguchi Grey Relational Analysis

B. Magamai Radj

svcetmagimairaj@gmail.com

Sri Venkateshwaraa College of Engineering & Technology

Sendhil Kumar Natarajan

National Institute of Technology Puducherry, Union Territory of Puducherry

Gopi Vasudevan

National Institute of Technology Puducherry, Union Territory of Puducherry

Research Article

Keywords: Dissimilar material, Mechanical strength, multi-response optimization

Posted Date: April 30th, 2024

DOI: https://doi.org/10.21203/rs.3.rs-4309268/v1

Additional Declarations: No competing interests reported.

Multi-Response Optimization of Process Parameters in Friction Stir Welding of AA 8011-H14 / AA 5052-H34 using Taguchi Grey Relational Analysis

B. Magamai Radj[1*], Sendhil Kumar Natarajan[2], Gopi Vasudevan[3].

[1*]Department of Mechanical Engineering, Sri Venkateshwaraa College of Engineering & Technology, Puducherry, India.

[2,3]Department of Mechanical Engineering, National Institute of Technology Puducherry, Karaikal, Union Territory of Puducherry, – 609609, India.

ABSTRACT

Friction stir welding (FSW) offers a distinct advantage in its ability to effectively join dissimilar metals and alloys. This study focuses on the butt welding of AA 8011-H14 and AA5052-H34 through FSW, aiming to explore the influence of process parameters on crucial mechanical properties such as ultimate tensile strength, yield strength, percentage elongation, and hardness. The examination of the welded cross-section revealed variations in both grain orientation and size across different zones. Notably, most failures were identified at the base of AA8011-H14 on the Advancing side. Furthermore, the hardness of the nugget zone exhibited variability based on the material ratio mix, with the maximum hardness observed on the AA5052-H34 side. Comparisons of optimal joint efficiencies were made to assess the overall effectiveness of the welded joints. This investigation contributes valuable insights into the intricacies of FSW when applied to dissimilar metal combinations, shedding light on the impact of process parameters on the mechanical characteristics of the joints.

Keywords: Dissimilar material, Mechanical strength, multi-response optimization

*Corresponding author: B. Magamai Radj, E-Mail: svcetmagimairaj@gmail.com.

Mobile: + 91 9677835595.

1. Introduction

Welding stands as a fundamental manufacturing procedure employed to create components or assemblies possessing substantial strength within a short time frame[1]. Nevertheless, the FSW process frequently experiences challenges associated with reduced precision and extended testing cycles, affecting its overall performance[2]. Aluminum alloys boast numerous advantages, including high strength, low density, excellent corrosion resistance, superior formability, and a lightweight composition [3]. In fusion welding, the need for a high rate of heat input arises

due to the higher thermal conductivity of aluminum alloys compared to steel. Additionally, conventional fusion welding processes demand preheating [4, 5]. To address the challenges posed by traditional fusion welding methods, FSW has been extensively utilized in various industrial sectors, including aerospace, automotive, and shipbuilding industries[6]. The Al-Mg (5XXX) series, classified as non-heat-treatable aluminum alloys, find practical applications in marine and aerospace industries owing to their outstanding corrosion resistance and high-strength characteristics[7, 8]. This can be credited to the exceptional mechanical properties of aluminum, which encompass a high strength-to-weight ratio, low density, outstanding corrosion resistance, ease of fabrication, and recyclability[9, 10]

Moreover, these dissimilar FSW processes effectively address issues encountered in other fusion welding methods, such as segregation, heat-affected zone (HAZ) liquation cracking, and the formation of brittle intermetallic[11]. FSW proves advantageous by eliminating the need for highly skilled labor, preheating of metals, and the complexity associated with filler material, commonly present in conventional fusion welding processes[12, 13]. Traditional fusion welding methods often fall short in achieving high-strength welded joints, especially when dealing with dissimilar aluminum materials[14]. The non-heat-treatable 5XXX Al alloys, known for their exceptional corrosion resistance and high-strength properties, find suitability in marine and aerospace applications. Employing the FSW process becomes crucial in minimizing defects and ensuring effective welding of these alloys[7, 15].

Research has indicated that employing the design of experiments methodology is effective in optimizing fusion joints of dissimilar alloys through FSW, incorporating various combinations of input parameters in the joining process[16]. Notably, the US Coast Guard utilizes AA5456 for wall structures, deck floors, and rescue boats[15]. Koilraj et al. [11] conducted experiments to join dissimilar combinations of AA2219-T87 and AA5083-H321 using FSW, employing Taguchi's design approach to optimize parameters for achieving maximum tensile strength. This resulted in a 90% joint efficiency, with most failures occurring at the HAZ. In another study, Şefika Kasman[17] experimented with dissimilar FSW joining of AA6082/AA5754 aluminum alloys, utilizing multi-response optimization of process parameters through Taguchi's design matrix and L9 orthogonal array. The achieved joint efficiency for this dissimilar welding was 66% for AA6082 and 92% for AA5754 under optimum conditions.

Additionally, Şefika Kasman and Zafer Yenier[18]employed FSW methods to fabricate AA5754/AA7075 plates (5 mm thickness) and assessed the output results of ultimate tensile strength (UTS), Yield Strength (YS), percentage elongation (%E), and hardness (HR). Yi et al. [19] utilized a calorimetric technique, incorporating multiple regression analysis to quantify the relationships between heat input and grain size for Al 1100 and 5083. The selection of process parameters plays a crucial role in welding dissimilar materials, influencing the metal flow and proper material mixing at the nugget zone (NZ). These FSW parameters significantly impact joint efficiency and the occurrence of defects [20, 21].

Based on the literature survey, there is currently no reported instance of FSW between AA8011-H14 and AA5052-H34. Furthermore, there is a noticeable absence of papers addressing the multi-objective optimization of FSW processes and their diverse output responses. To minimize the number of experiments, this study employs the Taguchi L_9 orthogonal array in conjunction with Grey Relational Analysis for dissimilar materials (AA8011-H14 to AA5052-H34). The objective is to predict and optimize friction stir welding process parameters, aiming to achieve desired output responses, including ultimate UTS, YS, %E, and HR values across various cross-sectional welded regions. The chemical compositions and mechanical properties of the materials are detailed in Table *1* and Table *2*, respectively.

Table 1 Chemical composition (Wt %) of base metal used in this study

Material	**Si**	**Fe**	**Cu**	**Mn**	**Mg**	**Cr**	**Zn**	**Sn**	**Ni**	**Ti**	**Al**
AA5052-H34	0.231	0.466	0.056	0.034	2.690	0.172	0.125	0.115	0.012	0.014	Bal
AA8011-H14	0.43	0.84	0.14	0.22	0.16	0.03	0.16	0.135	0.000	0.02	Bal

Table 2 Mechanical properties of parent metals

Materials	**UTS (MPa)**	**YS (MPa)**	**E (%)**	**HR (Hv)**
AA5052-H34	257	181	13.18	83
A8011-H14	147	136	11.67	49.2

2. Experimental details

The welding process utilized a non-consumable rotating tool, featuring a 12mm diameter shoulder, a 4mm pin diameter, and a cylindrical pin profile with a length of 1.8mm, constructed from High-Speed Steel (HSS) M35 grade. The investigation utilized distinct aluminum materials, specifically 2mm thick sheets of AA8011-H14 and AA5052-H34. The AA8011-H14 sheets were situated on the advancing side (AS), whereas the AA5052-H34 sheets

were positioned on the retreating side (RS). The tool tilt angle was maintained at 0 degrees to the faying surfaces, and the tool rotation was set in the clockwise direction. This study focused on three key FSW input parameters: tool rotational speed, welding speed (traversing speed), and plunging depth, as detailed in Table *3*, including their levels, units, and notations. Taguchi's L9 experimental design matrix and its corresponding output responses are presented in Table *4*. For all output responses in this research (UTS, YS, %E, and HR) the criteria were set as "larger the better" to evaluate the effectiveness of the FSW joints.

Table 3 Process parameters of FSW and their levels

Welding parameters	**Unit**	**Level 1**	**Level 2**	**Level 3**
Tool rotational speed (N)	rpm	900	1100	1300
Welding speed (S)	mm/min	26	34	42
Plunge depth (P)	mm	0.06	0.10	0.14

Table 4 Taguchi's experimental design matrix and its output responses.

Expt. No.	**Input parameters**			**Output performance results**			
	N (rpm)	**S (mm/min)**	**P (mm)**	**UTS (MPa)**	**YS (MPa)**	**% E**	**HR at NZ (HV)**
1	900	26	0.06	151	149	5.53	64.5
2	900	34	0.10	161	145	4.80	68.1
3	900	42	0.14	147	141	4.73	63.1
4	1100	26	0.10	175	169	9.96	71.9
5	1100	34	0.14	173	161	8.50	65.6
6	1100	42	0.06	163	147	5.80	62.3
7	1300	26	0.14	155	153	8.70	74.2
8	1300	34	0.06	153	139	5.00	69.8
9	1300	42	0.10	154	142	7.90	72.7

3. Results and discussion

3.1 Mechanical Properties

Transverse tensile specimens were prepared by the ASTM E8 standard [22], as illustrated in Figure *1*. The joint efficiency for the optimally welded joint was computed by considering the mechanical properties of both AA8011-H14 and AA5052-H34 base metals. The findings depicted Figure *2* indicate that the joint efficiency of AA8011 surpasses that of AA5052 in terms of mechanical properties.

Figure 1 Tensile specimen after testing

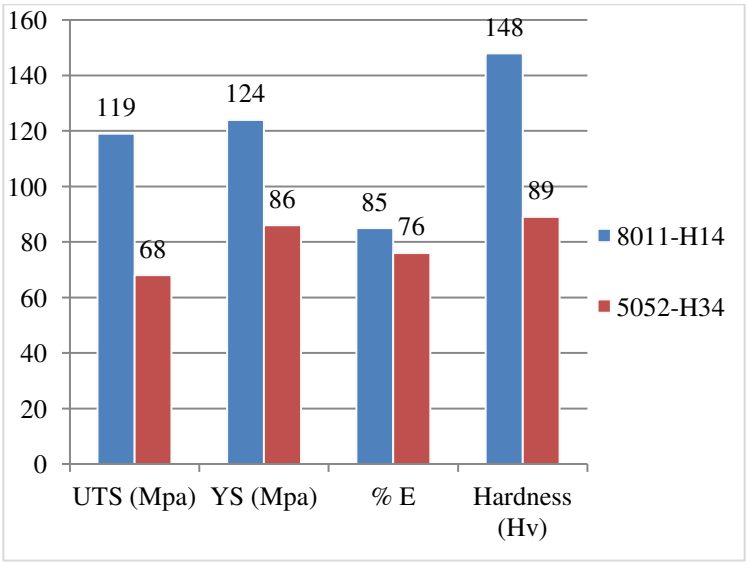

Figure 2 Joint efficiency of AA8011-H14 and AA 5052-H34 on mechanical properties.

3.2 Influence of FSW parameters on ultimate tensile strength

The impact of FSW process parameters (N, S, P) on UTS is depicted in the response contour plot shown in Figure *3* (a-c). As illustrated in Figure 3(a), an increase in tool rotational speed from 900 rpm to 1100 rpm corresponds to an increase in UTS; however, beyond 1100 rpm, the UTS value starts to decrease. Figure 3(b) indicates that an increase in both tool rotational speed and plunging depth leads to an elevation in UTS, reaching a maximum at an intermediate level. Further increases in tool rotational speed and plunging depth result in a subsequent decrease in UTS. Additionally, it is observed that an increase in welding speed contributes to a decrease in UTS, and reducing welding speed further enhances the maximum tensile strength, as shown in Figure 3(a) and (c).

In FSW, the key factors influencing the tensile strength and fracture location of joints are primarily determined by the tool rotational speed, with other parameters following in significance. Tensile testing has revealed that joints are prone to breaking at defective zones, such as tunnels, pinholes, and cracks, within the weldments. Conversely, defect-free joints tend to fail in regions characterized by lower hardness. At lower tool rotational speeds (900 rpm), higher welding speeds (42 mm/min), and plunging depths (0.14 mm), the welded zone is susceptible to tunnel defects due to the insufficient generation of frictional heat, as depicted in Figure 3(b). The combined effect of welding speed and plunging force in the FSW process significantly contributes to achieving higher tensile strength, as evident in Figure 3(c), where moderate levels of these two parameters result in elevated UTS values. Optimal process parameters play a crucial role in influencing excellent high-strength joints and ensuring better weld quality. The tensile strength of the aluminum alloy weldments exhibits a proportional relationship with the welding travel speed [23].

In FSW joints, lower heat generation occurs at higher welding speeds, leading to a faster rate of cooling. Consequently, during welding, metallurgical transformations such as coarsening of precipitates, re-precipitation, and solubilization are reduced, resulting in weaker welded joints [24]. On the other hand, tensile strength decreases with an increase in plunging depth beyond 0.1 mm (Figure 3(c)). It is observed that forcing the plunging depth beyond a critical point leads to thinning and material wearing out at the nugget zone, gradually reducing tensile strength.

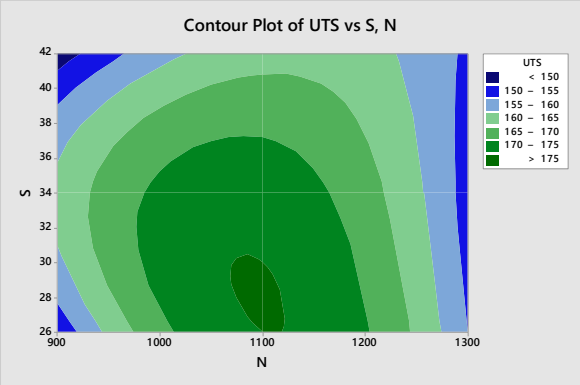

Fig. 3 (a)

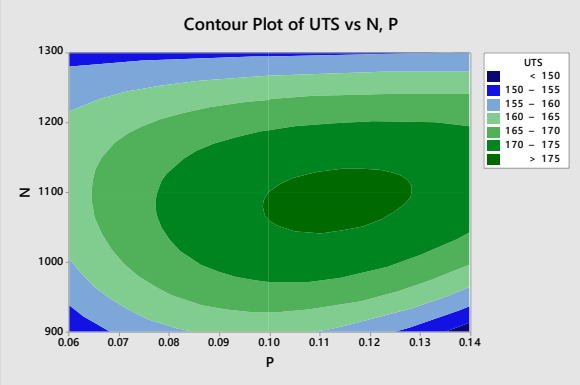

Fig..3 (b)

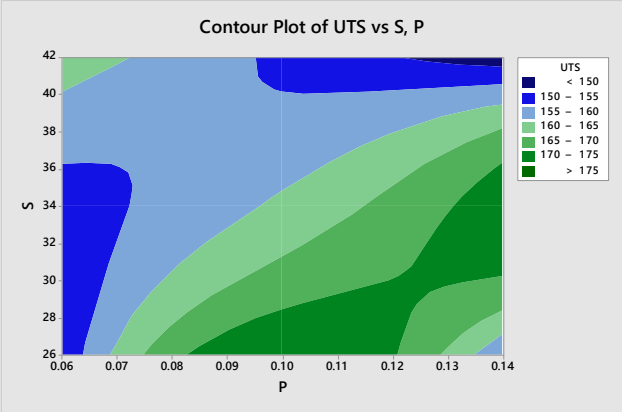

Fig..3 (c)

Figure 3 Contour graph exhibits the effect of FSW parameters on UTS of dissimilar joints (AA8011-H14 /AA 5052-H34).

3.3 Effect of FSW parameters on yield strength

In this investigation, the reduction in YS is linked to insufficient generation of frictional heat, leading to the formation of defects. According to Kim et al.[25], a deficiency in heat input, resulting from reduced frictional effects at the NZ, contributes to the occurrence of tunnel defects, cavities, and groove defects. The diminished heat input, associated with higher welding speed, causes a decrease in the flow ability of the plasticized material at the weld zone[26]. The contour graph illustrating YS is presented in Figure *4* (a-c). Figure 4(a) indicates that deviations from the optimal FSW tool rotational speed (1100 rpm) lead to a decrease in YS. An increase in rotational speed, when combined with welding speed, induces excessive turbulence and inadequate material coalescence, resulting in lower YS and tunnel defects (Figure 4(b)). Furthermore, an increase in welding speed contributes to a decrease in YS due to lower heat input. Similarly, the maximum YS is achieved at a plunging depth of 0.10 mm (Figure 4(b)). Any further increase or decrease in plunging depth beyond the optimal level (0.10 mm) results in a decrease in YS strength. Figure 4(c) highlights the optimal levels of plunging depth and tool rotational speed at 0.10-0.12 mm and 1100 rpm, respectively, for attaining maximum yield strength.

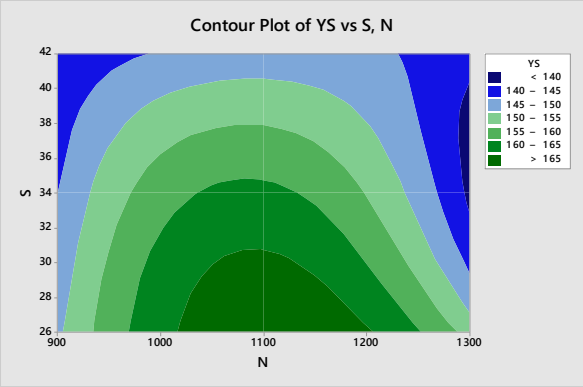

Fig. 4 (a)

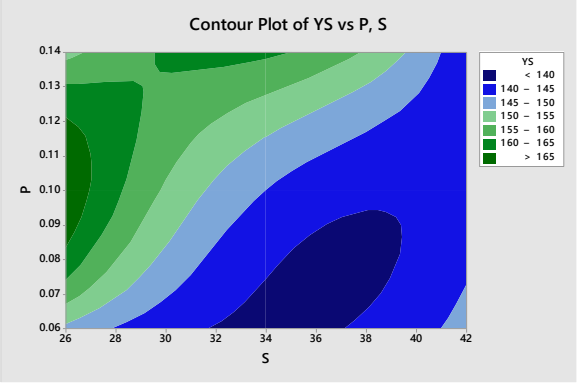

Fig.4 (b)

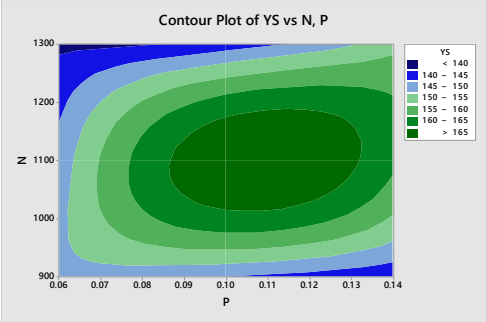

Fig. 4 (c)

Figure 4 Contour plot of process parameters on YS of the dissimilar joint (AA8011-H14 / AA 5052- H34).

3.4 Effect of FSW parameters on percentage elongation

Table 4 presents the results of %E, while the contour plots are illustrated in Figure *5*(a-c). Observing Figure 5(a), it becomes apparent that an increase in plunging force and tool rotational speed corresponds to an increase in the %E. However, beyond the optimal levels indicated in Figure 5(a), a decreasing trend in %E is observed as these parameters continue to increase. Figure 5(b) reveals that an increase in tool rotational speed and a decrease in welding speed result in higher %E. This enhanced %E is attributed to the combination of lower traveling speed and higher tool rotational speed, leading to increased heat input and proper material flow with a fine-grain structure (Figure 8(a)). In tensile tests, the %E is directly proportional to plastic deformation, correlating with grain properties. Fine grain refinement and dynamic recrystallization during the FSW process contribute to improved metal flow. Additionally, as tool rotational speed and plunging depth increase, the friction between the base metal and tool shoulder on the faying surface of the sheet also increases. This leads to dynamic recrystallization in the FSW region, enhancing %E through

improved plastic deformation[23]. Figure 5(c) highlights that the optimal parameter settings of 0.10–0.13 mm plunging depth and 26 mm/min welding speed result in a higher range of %E.

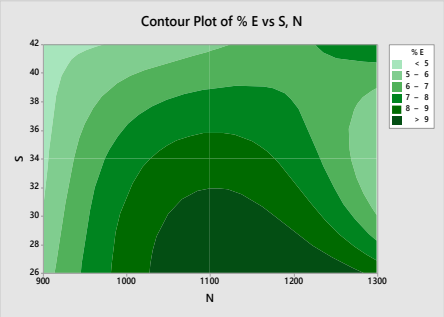

Fig. 5 (a)

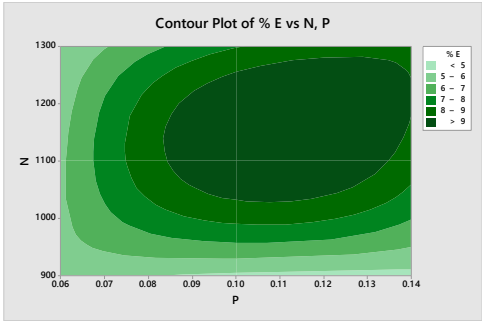

Fig. 8 (b)

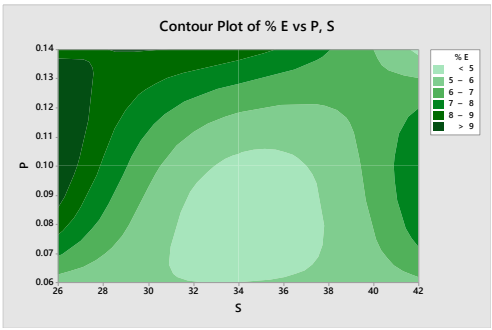

Fig. 5 (c)

Figure 5 Contour plot of process parameters on %E of the dissimilar joint (AA8011-H14/ AA 5052-H34).

3.5 Hardness distribution of FSW of dissimilar joints

In this investigation, hardness measurements were conducted at various zones within the cross-sectional FSW samples, including the base metal (BM), advancing side of the heat-affected zone (ASHAZ), advancing side of the thermo-mechanically affected zone (ASTMAZ), NZ, retreating side of the thermo-mechanically affected zone (RSTMAZ), and retreating side of the heat-affected zone (RSHAZ). The results are depicted in Figure *6*. Notably, the microhardness values exhibit an increasing trend towards the retreating side (AA 5052-H34), while lower hardness values are consistently observed on the AA 8011-H14 side (AS) across all joints. Microhardness measurements taken at ASHAZ and ASTMAZ show considerably lower hardness values. Conversely, higher hardness values are recorded

on the retreating side (RS) represented by AA 5052-H34. The hardness values within the stir zone vary due to the mechanical mixing ratio at the interfaces of two distinct materials. Microhardness values at the NZ are higher compared to the heat-affected zone (HAZ) of the advancing side, attributable to finer grain size. The heat input in the stir zone influences the volume mix of materials based on their plastic flow rate. Hardness values in the thermo-mechanically affected zones (TMAZ) range between 56 Hv and 65 Hv. Specifically, at the FSW joint, 56 Hv is measured on the AA 8011-H14 side, while 65 Hv is recorded on the AA 5052-H34 side. However, exceeding the optimum levels of tool rotational speed, welding speed, and plunging force leads to excessive heat generation at the stir zone, resulting in grain coarsening and a decrease in NZ hardness.

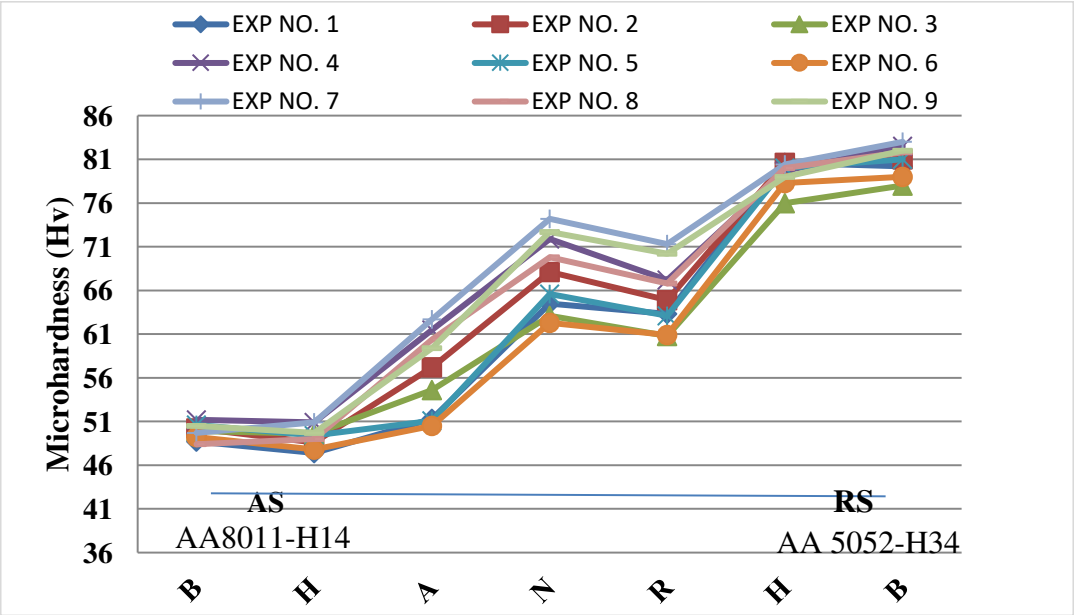

Figure 6 Hardness profile of all the FSW dissimilar joints (AA 8011-H14/AA5052-H34).

4 Metallurgical Behavior of FSW Joint

4.1 Microstructural analysis

Metallographic specimens from friction stir-welded joints, including the NZ, TMAZ, HAZ, and BM on both sides AS and RS, were meticulously prepared and examined for microstructure analysis using an optical metallurgical microscope. The microstructure of the two dissimilar parent metals, each with distinct grades, is illustrated in Figure *7* (a) and (b). In both base metals, large elongated grains are observed along the rolling direction. The welded joint is characterized by three distinct regions: the NZ, TMAZ, and HAZ, present on both sides of the adjoining edge. The

microstructural features within these regions were carefully examined to gain insights into the material properties and structural changes resulting from the FSW process.

Fig. 7 (a)

Fig. 7(b)

Figure 7 Microstructure of base metals (a) AA8011-H14 (b) AA5052-H34.

Figure *8* (a-d) highlight distinctions among various cross-sectional regions in the welded specimens, resulting from plastic deformation induced by frictional heat and grain orientation. In Figure 8(a), the NZ is depicted, showcasing equiaxed grains formed through dynamic recrystallization triggered by sufficient heat generation during the welding process. Moving to Figure 8(b), the interface zone between the TMAZ and NZ is presented, revealing variations in grain structure and boundaries at the intermetallic component (IMC) layer of dissimilar metals.

Figure 8(c) provides insight into the microstructure, displaying grain variations and boundaries within the TMAZ, which has undergone deformation and elongation due to the rotational movement and pressure applied by the welding tool. This deformation is a result of strain and intense plastic deformation, leading to discernible differences in grain size between the NZ and TMAZ. The orientation and size of grains in the TMAZ differ from those observed in the NZ. Examining Figure 8(d), the HAZ is presented, revealing a grain structure unaffected by the tool pin movements. The grain structure in the HAZ appears overgrown compared to the TMAZ and NZ, resembling that of the base metal. This indicates that the mechanical impact of the tool on the HAZ is less pronounced, allowing the grain structure to retain characteristics more similar to the original base metal.

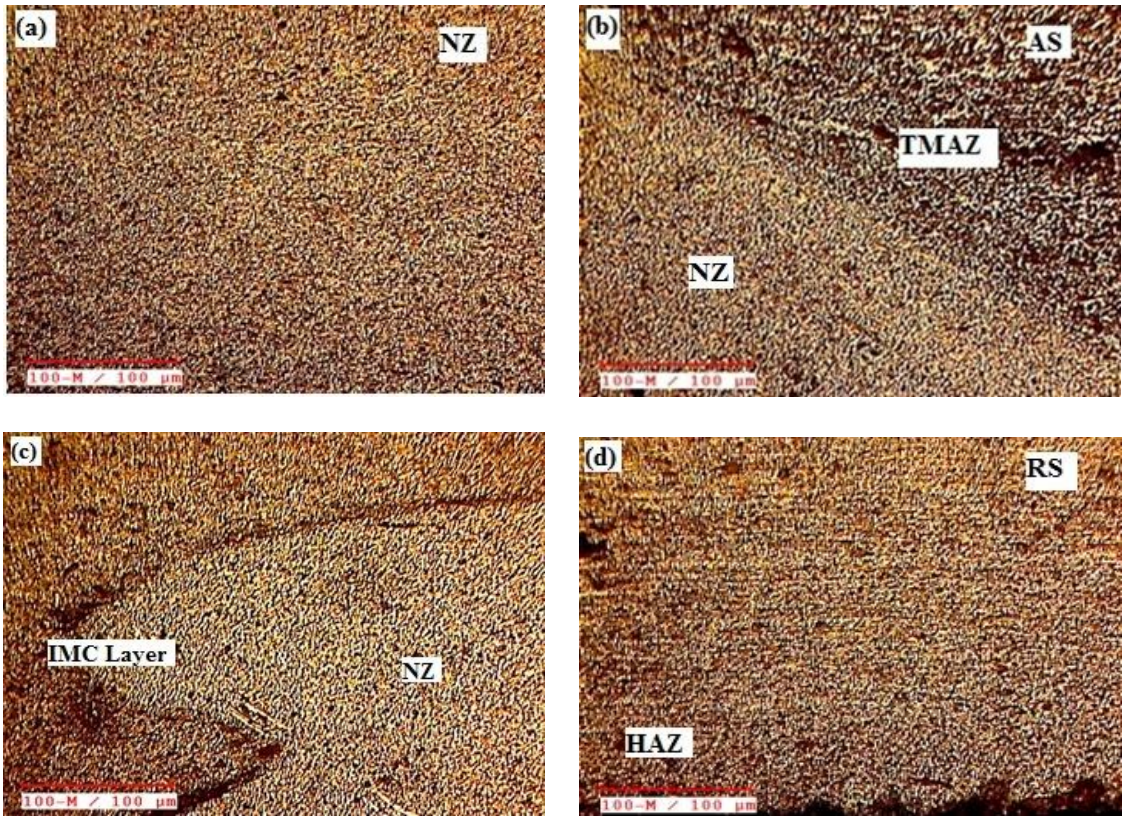

Figure 8 Microstructure of various cross-sectional regions depicts FSW joints (a) NZ (b) Interface between TMAZ and NZ (c) IMC layer at NZ (d) HAZ.

4.2 Macro structural analysis

The macrostructure of the welded specimens is depicted in Figure *9* (a-c), where the white and dark shaded zones correspond to 5052-H34 at the RS and 8011-H14 at the AS, respectively. Macrostructure observations of the FSW joints reveal that defect-free welding is contingent upon optimal process factors. As shown in Figure 9(a), it can be concluded that a defect-free welded zone was achieved when the joint was welded at a tool rotational speed of 1100 rpm, a welding speed of 26 mm/min, and a plunging depth of 0.1 mm. This may account for the higher tensile strength and YS properties achieved in this particular joint.

Figure 9(b) depicts a tunnel-like defect and weld collapse at the bottom of the stir zone. This is attributed to insufficient heat input and a transformation of metal flow, occurring at a lower tool rotational speed of 900 rpm, higher welding speed of 42 mm/min, and a greater plunging depth of 0.14 mm. Likewise, in Figure 9(c), at 1300 rpm, 34 mm/min welding speed, and 0.06 mm plunging depth, an observation of a tunnel and wormhole-like defect at the bottom is noted. This may be a result of excessive turbulence caused by a higher tool rotational speed and welding speed. It was found that inadequate material flow at the bottom of the stir zone was due to the lower plunging depth

(Figure 9(c)). Figures 9(a-c) collectively demonstrate that a proper ratio of mechanical mixing of materials occurred in the welded zone for almost all the FSW joints, emphasizing the importance of process parameters in achieving defect-free welds and desirable mechanical properties.

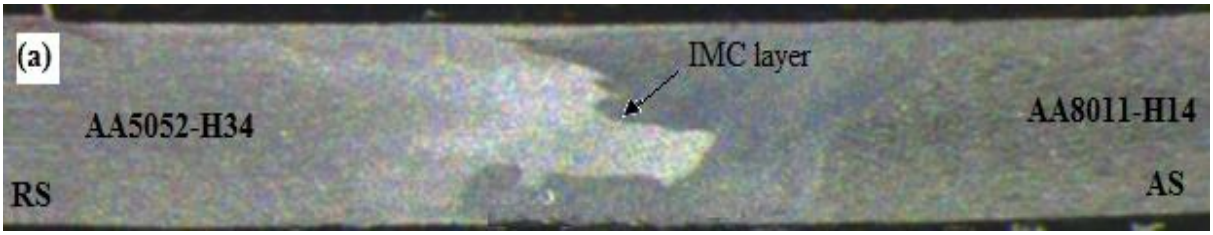

Fig. 9 (a) Defect-free joint.

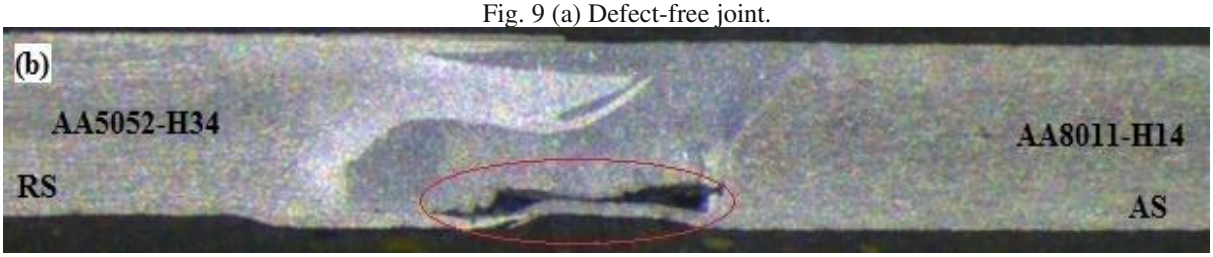

Fig.9 (b) Long tunnel defect at the bottom of NZ.

Fig.9 (c) Tunnel defect and wormhole.

Figure 9 Cross-sectional macro structure of FSW dissimilar joints (AA8011-H14/AA5052-H34).

5 Multi-Objective Optimization using Grey-Based Approach

5.1 Implementation of Taguchi Grey Relational Analysis for experimental data

In this research, the Taguchi method, in conjunction with Grey Relational Analysis (GRA), was employed to address and analyze multiple output responses, including UTS, YS, %E, and microhardness (Hv). The experimental data obtained from these output responses were initially normalized from zero to one[27, 28]. The data sequences for UTS, YS, %E, and Hv values in the FSW joints were treated as criteria for performance characteristics, employing a "larger the better" perspective. The normalization process was implemented to facilitate meaningful comparisons and analyses across the various performance criteria.

$$x_i^*(k) = \frac{x_i(k) - \min x_i(k)}{\max x_i(k) - \min x_i(k)} \quad (1)$$

After generating grey relational values, Where $x_i^*(k)$ the value after the grey relational generation, $\min x_i(k)$ is the smallest value $x_i(k)$ for the k^{th} response and $\max x_i(k)$ is the largest value $x_i(k)$ for the k^{th} response. i = 1–9 is the number of experiments and k = 1–4 is the number of output responses. After data processing, all the sequences using Equation (1) are listed in Table *5*

Table 5 Normalized values of output responses of dissimilar FSW joint (AA8011-H14/AA5052-H34).

Expt. No.	UTS	YS	% E	Micro HR(Hv)
1	0.143	0.333	0.153	0.184
2	0.500	0.200	0.013	0.487
3	0	0.066	0	0.067
4	1	1	1	0.807
5	0.929	0.733	0.721	0.277
6	0.571	0.267	0.205	0
7	0.286	0.467	0.759	1
8	0.214	0	0.052	0.630
9	0.250	0.100	0.606	0.874

After computing normalized values, the calculation of grey relational coefficients (GRCs) $\xi_i(k)$ as illustrated in, was carried out as follows [28, 29]:

$$\xi_i(k) = \frac{\Delta \min + \zeta.\Delta \max}{\Delta 0i(k) + \zeta.\Delta \max} \tag{2}$$

Where $\Delta_{0i}(k) = \left|x_0^*(k) - x_i^*(k)\right|$ are the deviation sequence of the reference sequence $x_0^*(k)$ and the comparability sequence $x_i^*(k)$, $\Delta \max(k)$, and $\Delta \min(k)$ are the largest and smallest values of $\Delta_{0i}(k)$ and ζ is the distinguishing or identification coefficient. If equal preferences are given to all parameters, then ζ is taken as 0.5. The GRC for each experiment of the L_9 orthogonal array was calculated using Equation (2) and is given in Table *6*.

After calculating the grey relational coefficients, grey relational grades (GRGs) were computed which is the mean sum of the GRCs by using Equation (3)[28, 29]:

$$\gamma i = \frac{1}{n}\sum_{k=1}^{n}\xi i(k) \tag{3}$$

Where γ_i is the GRG for the i^{th} experiment and n is the number of performance characteristics. Table 6 presents the GRGs for the output performance characteristics along with their corresponding rankings.

Table 6 Calculated GRC and GRG with its ranking.

Expt. No.	GRC				GREG (γ_i)	Ranking
	UTS ξ_i (1)	YS ξ_i (2)	% E ξ_i (3)	HR at NZ ξ_i (4)		
1	0.368	0.428	0.371	0.379	0.387	8
2	0.500	0.385	0.336	0.493	0.429	5
3	0.333	0.347	0.333	0.349	0.341	9
4	1	1	1	0.722	0.930	1
5	0.876	0.652	0.642	0.409	0.645	2
6	0.538	0.406	0.386	0.333	0.415	6
7	0.412	0.484	0.675	1	0.643	3
8	0.389	0.333	0.345	0.575	0.410	7
9	0.400	0.357	0.559	0.799	0.529	4

5.2 Analysis of GRG with ANOVA and response plots

Following data preprocessing, the GRC is determined, and the GRC values are averaged. The resulting GRG is computed and ranked, as illustrated in Table 6. Mean effects for each parameter level, along with their rankings, are calculated and presented in Table 7. These values are also visually represented Figure *10*. The optimal process parameters for FSW were determined based on the higher GRG values. Experiment No. 4 emerged as the top-ranking configuration, featuring a tool rotational speed of 1100 rpm, welding speed of 26 mm/min, and plunging depth of 0.10 mm. The optimal parameter settings for enhanced output responses, denoted as (N_2, S_1, P_2), are detailed in Table *7*. To examine the contributions of each process factor to the GRG, ANOVA was employed, and the results were presented Table 8.

Table 7 Table displaying the GRG responses

Level	GREG		
	N	S	P
1	0.3857	0.6533*	0.4040
2	0.6633*	0.4947	0.6293*
3	0.5273	0.4283	0.5430
Delta	0.2777	0.2250	0.2253
Rank	1	3	2

*****Optimal level of factors

ANOVA breaks down the overall variability into the individual contributions of each process parameter and the associated error. The results obtained from ANOVA, as depicted in Table 8, reveal that the tool rotational speed stands out as the most influential parameter, contributing significantly with a 41.33% impact. Following closely, the welding speed and plunging depth contribute 28.66% and 27.71%, respectively, towards enhancing the output

responses. These findings highlight the relative importance of each process parameter in influencing the overall variability and improving the performance characteristics of the FSW process.

Figure 10 Response plot for a grey relational grade.

Table 8 ANOVA results for GRG.

Source	DF	Adj SS	Adj MS	*F*-value	*P*-value	Contribution (%)
N	2	0.115664	0.057832	18.10	0.052	41.33
S	2	0.080200	0.040100	12.55	0.074	28.66
P	2	0.077550	0.038775	12.14	0.076	27.71
Error	2	0.006390	0.003195	–	–	02.28
Total	8	0.279804	–	–	–	–

5.3 Predicted Optimum Condition

From the experiments, it was observed that the optimum level settings are $N_2S_1P_2$ (Table 7). So, the predicted GRG $\hat{\gamma}$ can be calculated by Equation (4).

$$\hat{\gamma} = \gamma_m + \sum_{i=1}^{q}(\overline{\gamma}_i - \gamma_m) \tag{4}$$

The predicted GRG is 0.896 according to Equation 4, while the observed GRG at the optimum condition is 0.930. The negligible difference of only 0.034 supports the notion that any potential error is minimal. Therefore, following the perspective advocated by Kesharwani et al.[30], as the optimal parameter setting already exists in the design matrix, there is no imperative need for a confirmation experiment. The present analysis reveals that the optimization of the complex multiple performance characteristics in FSW of dissimilar metals AA8011-H14 and AA

5052-H34 has been effectively translated into the optimization of a single GRG, streamlining the evaluation and decision-making process.

Conclusion

In this current investigation, the impact of FSW process parameters, specifically tool rotational speed, welding speed, and plunging depth, on the mechanical properties (UTS, YS, %E, and HV) of dissimilar aluminum alloys (AA 8011-H14 and AA 5052-H34) was thoroughly examined to maximize joint efficiency.

1. A robust joint was successfully achieved by employing a tool rotational speed of 1100 rpm, welding speed of 26 mm/min, and plunging depth of 0.10 mm. These optimized FSW joints demonstrated impressive mechanical properties, with maximum UTS, YS, and %E values reaching 175 MPa, 169 MPa, and 9.96, respectively. Across the nine experiments conducted, UTS ranged from 175 MPa to 147 MPa, YS varied between 169 MPa and 139 MPa, and %E showed a range from 9.96 to 4.73.
2. Contour plot analysis revealed that the optimal conditions for maximizing UTS, YS, and %E were a tool rotational speed and plunging depth of 1100 rpm and 0.1 mm, respectively. Deviations from these optimal values resulted in a decrease in joint strength, while a lower welding speed contributed to increased joint strength.
3. The hardness behavior exhibited distinct patterns, influenced by the formation of a stirred zone and fine grain structure. The highest hardness value (74.2 Hv) was attained on the AA5052-H34 side under specific conditions (tool rotational speed of 1300 RPM, welding speed of 26 mm/min, and plunging depth of 0.14 mm).
4. Macrostructure analysis confirmed proper mixing of materials in all welded specimens. Defects such as wormholes and tunnels were observed in the stir zone of joints, except under the optimized welding parameters, which produced higher welding strength.
5. GRA identified the maximum GRG value of 0.930 in Experiment No. 4 (tool rotational speed: 1100 rpm, welding speed: 26 mm/min, plunging depth: 0.10 mm), ranking it first.
6. ANOVA results demonstrated the significant impact of all selected process parameters on GRG values, with tool rotational speed contributing the most at 41.33%, followed by welding speed at 28.66%, and plunging depth at 27.71%.

In conclusion, this study successfully demonstrated the feasibility of the FSW process on dissimilar AA 8011-H14 / AA 5052-H34 2-mm thickness sheets, utilizing the Taguchi GRA method to address multi-response optimization challenges.

Declarations

Ethics approval and consent to participate: Not applicable

Consent for Publication: Not applicable

Availability of data and materials: The datasets used and/or analyzed during the current study are available from the corresponding author on reasonable request

Competing interests: The authors declare that they have no competing interests.

Funding: Not applicable

Credit authorship contribution statement:

B. Magamai Radj: Conceptualization, Validation, Resources, Writing - Review & Editing, Supervision, Project administration.

Sendhil Kumar Natarajan: Conceptualization, Validation, Resources, Writing - Review & Editing, Supervision, Project administration.

Gopi Vasudevan: Conceptualization, Formal analysis, Investigation, Data Curation, Visualization, Writing - Original Draft.

References

1. Uppada Sudhakar and Suraparaju SK and BMVAR and NSK (2020) Optimization of Process Parameters in Resistance Spot Welding Using Artificial Immune Algorithm. In: Deepak BBVL. and Parhi D and JPC (ed) Innovative Product Design and Intelligent Manufacturing Systems. Springer Singapore, Singapore, pp 477–485

2. Yu F, Zhao Y, Lin Z, et al (2023) Prediction of Mechanical Properties and Optimization of Friction Stir Welded 2195 Aluminum Alloy Based on BP Neural Network. Metals (Basel) 13:. https://doi.org/10.3390/met13020267

3. Taban E, Kaluc E (2006) Microstructural and mechanical properties of double-sided MIG, TIG and friction stir welded 5083-H321 aluminium alloy

4. Pandey S, Wattal R, Garg G, Agakhani M (2002) Recent trends in welding of Aluminium. In: Workshop organized by the Aluminium Association of India and Indian Institute of Metals, Chandigarh, February

5. Introduction

6. Kim D, Lee W, Kim J, et al (2010) Formability evaluation of friction stir welded 6111-T4 sheet concerning joining material direction. Int J Mech Sci 52:612–625. https://doi.org/10.1016/j.ijmecsci.2010.01.001

7. Chionopoulos SK, Sarafoglou CHI, Pantelis DI, Papazoglou VJ (2008) Effect of tool pin and welding parameters on friction stir welded (FSW) marine aluminum alloys. In: Proceedings of the 3rd international conference on manufacturing engineering (ICMEN). pp 1–3

8. Kallee S (2000) Application of friction stir welding in the shipbuilding industry. In: Proceedings

9. Mazlan S, Yidris N, Koloor SSR, Petrů M (2020) Experimental and numerical analysis of fatigue life of aluminum al 2024-t351 at elevated temperature. Metals (Basel) 10:1–14. https://doi.org/10.3390/met10121581

10. Shokravi H, Mohammadyan-Yasouj SE, Koloor SSR, et al (2021) Effect of alumina additives on mechanical and fresh properties of self-compacting concrete: A review. Processes 9:. https://doi.org/10.3390/pr9030554

11. Koilraj M, Sundareswaran V, Vijayan S, Koteswara Rao SR (2012) Friction stir welding of dissimilar aluminum alloys AA2219 to AA5083 - Optimization of process parameters using Taguchi technique. Mater Des 42:1–7. https://doi.org/10.1016/j.matdes.2012.02.016

12. Chien CH, Lin WB, Chen T (2011) Optimal FSW process parameters for aluminum alloys AA5083. In: Journal of the Chinese Institute of Engineers, Transactions of the Chinese Institute of Engineers, Series A. Taylor and Francis Ltd., pp 99–105

13. Dinaharan I, Murugan N (2012) Optimization of friction stir welding process to maximize tensile strength of AA6061/ZrB 2 in-situ composite butt joints. Metals and Materials International 18:135–142. https://doi.org/10.1007/s12540-012-0016-z

14. Vijayan S, Raju R, Rao SRK (2010) Multiobjective optimization of friction stir welding process parameters on aluminum alloy AA 5083 using Taguchi-based grey relation analysis. Materials and Manufacturing Processes 25:1206–1212. https://doi.org/10.1080/10426910903536782

15. Kallee S (2000) Application of friction stir welding in the shipbuilding industry. In: Proceedings

16. Shunmugasundaram, Kumar AP, Mishra D, et al (2021) A review on process parameter optimization of friction stir welded dissimilar alloys. In: AIP Conference Proceedings. American Institute of Physics Inc.

17. Kasman Ş (2013) Multi-response optimization using the Taguchi-based grey relational analysis: A case study for dissimilar friction stir butt welding of AA6082-T6/AA5754-H111. International Journal of Advanced Manufacturing Technology 68:795–804. https://doi.org/10.1007/s00170-012-4720-0

18. Kasman Ş, Yenier Z (2014) Analyzing dissimilar friction stir welding of AA5754/AA7075. International Journal of Advanced Manufacturing Technology 70:145–156. https://doi.org/10.1007/s00170-013-5256-7

19. Yi D, Onuma T, Mironov S, et al (2017) Evaluation of heat input during friction stir welding of aluminium alloys. Science and Technology of Welding and Joining 22:41–46. https://doi.org/10.1080/13621718.2016.1183079

20. Rajakumar S, Balasubramanian V (2012) Establishing relationships between mechanical properties of aluminium alloys and optimized friction stir welding process parameters. Mater Des 40:17–35. https://doi.org/10.1016/j.matdes.2012.02.054

21. Palanivel R, Koshy Mathews P, Murugan N, Dinaharan I (2012) Effect of tool rotational speed and pin profile on microstructure and tensile strength of dissimilar friction stir welded AA5083-H111 and AA6351-T6 aluminum alloys. Mater Des 40:7–16. https://doi.org/10.1016/j.matdes.2012.03.027

22. Committee ASMIH (1992) Properties and selection: nonferrous alloys and special-purpose materials. ASM international 2:1143–1144

23. Lee W-B, Yeon Y-M, Jung S-B Mechanical Properties Related to Microstructural Variation of 6061 Al Alloy Joints by Friction Stir Welding

24. Zhang Z, Wu Q, Grujicic M, Wan ZY (2016) Monte Carlo simulation of grain growth and welding zones in friction stir welding of AA6082-T6. J Mater Sci 51:1882–1895. https://doi.org/10.1007/s10853-015-9495-x

25. Kim YG, Fujii H, Tsumura T, et al (2006) Three defect types in friction stir welding of aluminum die casting alloy. Materials Science and Engineering: A 415:250–254. https://doi.org/10.1016/j.msea.2005.09.072

26. Sharma C, Dwivedi DK, Kumar P (2012) Effect of welding parameters on microstructure and mechanical properties of friction stir welded joints of AA7039 aluminum alloy. Mater Des 36:379–390. https://doi.org/10.1016/j.matdes.2011.10.054

27. Kasman Ş (2013) Multi-response optimization using the Taguchi-based grey relational analysis: a case study for dissimilar friction stir butt welding of AA6082-T6/AA5754-H111. The international journal of Advanced manufacturing technology 68:795–804

28. Ranganathan S, Senthilvelan T (2011) Multi-response optimization of machining parameters in hot turning using grey analysis. International Journal of Advanced Manufacturing Technology 56:455–462. https://doi.org/10.1007/s00170-011-3198-5

29. Sahu PK, Pal S (2015) Multi-response optimization of process parameters in friction stir welded AM20 magnesium alloy by Taguchi grey relational analysis. Journal of Magnesium and Alloys 3:36–46. https://doi.org/10.1016/j.jma.2014.12.002

30. Kesharwani RK, Panda SK, Pal SK (2014) Multi-Objective Optimization of Friction Stir Welding Parameters for Joining of Two Dissimilar Thin Aluminum Sheets. Procedia Materials Science 6:178–187. https://doi.org/10.1016/j.mspro.2014.07.022